



# VCU

Virginia Commonwealth University  
**VCU Scholars Compass**

---

Mechanical and Nuclear Engineering Publications

Dept. of Mechanical and Nuclear Engineering

---

2014

## Hybrid TiO<sub>2</sub> Solar Cells Produced from Aerosolized Nanoparticles of Water-Soluble Polythiophene Electron Donor Layer

Marshall L. Sweet

*Virginia Commonwealth University*

Joshua G. Clarke

*Virginia Commonwealth University*

Dmitry Pestov

*Virginia Commonwealth University*

Gary C. Tepper

*Virginia Commonwealth University*

James T. McLeskey Jr.

*Virginia Commonwealth University*, [jtmcleskey@vcu.edu](mailto:jtmcleskey@vcu.edu)

Follow this and additional works at: [http://scholarscompass.vcu.edu/egmn\\_pubs](http://scholarscompass.vcu.edu/egmn_pubs)

 Part of the [Mechanical Engineering Commons](#), and the [Nuclear Engineering Commons](#)

Copyright © 2014 Marshall L. Sweet et al. This is an open access article distributed under the Creative Commons Attribution License, which permits unrestricted use, distribution, and reproduction in any medium, provided the original work is properly cited.

---

Downloaded from

[http://scholarscompass.vcu.edu/egmn\\_pubs/30](http://scholarscompass.vcu.edu/egmn_pubs/30)

This Article is brought to you for free and open access by the Dept. of Mechanical and Nuclear Engineering at VCU Scholars Compass. It has been accepted for inclusion in Mechanical and Nuclear Engineering Publications by an authorized administrator of VCU Scholars Compass. For more information, please contact [libcompass@vcu.edu](mailto:libcompass@vcu.edu).

## Research Article

# Hybrid TiO<sub>2</sub> Solar Cells Produced from Aerosolized Nanoparticles of Water-Soluble Polythiophene Electron Donor Layer

Marshall L. Sweet,<sup>1</sup> Joshua G. Clarke,<sup>1</sup> Dmitry Pestov,<sup>2</sup>  
Gary C. Tepper,<sup>1</sup> and James T. McLeskey Jr.<sup>1</sup>

<sup>1</sup>Virginia Commonwealth University, Department of Mechanical and Nuclear Engineering, 401 West Main Street, Richmond, VA 23284, USA

<sup>2</sup>Virginia Commonwealth University, Nanomaterials Characterization Center, 601 West Main Street, Richmond, VA 23284, USA

Correspondence should be addressed to James T. McLeskey Jr.; [jtmcleskey@vcu.edu](mailto:jtmcleskey@vcu.edu)

Received 11 October 2013; Accepted 24 January 2014; Published 27 February 2014

Academic Editor: Paulo Fernandes

Copyright © 2014 Marshall L. Sweet et al. This is an open access article distributed under the Creative Commons Attribution License, which permits unrestricted use, distribution, and reproduction in any medium, provided the original work is properly cited.

Hybrid solar cells (HSCs) with water soluble polythiophene sodium poly[2-(3-thienyl)-ethoxy-4-butylsulfonate] (PTEBS) thin films produced using electrospray deposition (ESD) were fabricated, tested, and modeled and compared to devices produced using conventional spin coating. A single device structure of FTO/TiO<sub>2</sub>/PTEBS/Au was used to study the effects of ESD of the PTEBS layer on device performance. ESD was found to increase the short circuit current density ( $J_{sc}$ ) by a factor of 2 while decreasing the open circuit voltage ( $V_{oc}$ ) by half compared to spin coated PTEBS films. Comparable efficiencies of 0.009% were achieved from both device construction types. Current-voltage curves were modeled using the characteristic solar cell equation and showed a similar increase in generated photocurrent with an increase by two orders of magnitude in the saturation current in devices from ESD films. Increases in  $J_{sc}$  are attributed to an increase in the interfacial contact area between the TiO<sub>2</sub> and PTEBS layers, while decreases in  $V_{oc}$  are attributed to incomplete film formation from ESD.

## 1. Introduction

Hybrid solar cells (HSCs) consist of an inorganic semiconducting electron acceptor and an organic polymer electron donor sandwiched between a transparent conducting oxide anode and a metal cathode. Polymer-based solar cells have attracted considerable attention due to low production cost, solution processing, and an array of different materials suitable for device fabrication [1–3]. HSCs take advantage of the high electron mobilities (TiO<sub>2</sub>  $\approx$  0.001–10 cm<sup>2</sup> V<sup>-1</sup> s<sup>-1</sup>) [4, 5] in inorganic semiconductors to compensate for the poor hole mobilities in organic polymers (polythiophene polymers  $\approx$  0.00001–0.1 cm<sup>2</sup> V<sup>-1</sup> s<sup>-1</sup>) [6–9] which severely limit the electron diffusion length ( $\sim$ 10 nm) [10, 11]. The interface between the inorganic semiconductor and the organic polymer in HSCs must be within one diffusion length of exciton generation to effectively separate excitons

into holes and electrons. This presents a challenge to bilayer devices due to a limited interfacial contact area between the electron donor and acceptor layers. HSC devices have been designed with nanostructures (nanorods, nanoribbons, and interpenetrating layers) to increase the interfacial surface area [12–14].

An electrospray is a fine aerosol produced when electrical forces overcome surface tension forces in a liquid resulting in nebulization. While electrospray aerosols can be formed in a number of ways, the most common method is to apply a high electrical potential to a liquid inside of a metallic capillary tube. The liquid at the tip of the capillary forms a Taylor cone, formed by the competition between the electric force and surface tension. A fine jet of liquid is emitted from the tip of the Taylor cone and this jet breaks up into a fine aerosol of charged droplets [15]. The droplets may be on the order of 10's of nanometers and ideally can be controlled by

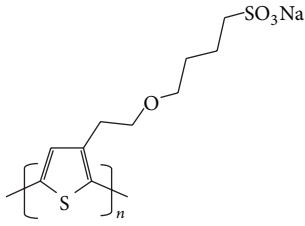


FIGURE 1: Molecular structure of PTEBS [36].

controlling the electric potential and solution properties [16]. Electrospray deposition (ESD) has become a viable technology for preparing polymer thin films of less than 100 nm from a precursor solution for organic photovoltaic devices [17–20] and for light-emitting diodes [21–23]. This technique offers several advantages towards large scale commercialization of organic photovoltaic devices over traditional spin coating for thin film deposition. ESD is inexpensive, efficient (minimal waste), and has a relatively high throughput [16] making it practical for large scale commercialization.

The polymers poly(3-hexylthiophene) [P3HT], poly(2-methoxy-5-(2-ethylhexyloxy)-p-phenylenevinylene) [MEH-PPV], and poly(3-octylthiophene) [P3OT] have widely been reported as electron donor materials in  $\text{TiO}_2$  HSCs [24–27]. These polymers are soluble in organic solvents such as toluene, chloroform, chlorobenzene, tetrahydrofuran, and xylene which are toxic in nature [28]. Commercialization of polymer based solar cells will require generation of several gigawatts of power [29], which corresponds to a solar cell (~5% efficient) area of thousands of square meters [30]. The toxicity of organic solvents makes them a poor option on this order of magnitude due to increased costs and difficulty of fabrication associated with environmental hazards. Water-soluble polymers are an obvious alternative due to water's prevalence, low cost, and safety. The water soluble-polymer sodium poly[2-(3-thienyl)-ethoxy-4-butylsulfonate] (PTEBS) (Figure 1) has been reported as an electron donor material in  $\text{TiO}_2$  HSCs by Qiao et al. [31–33] and in polymer solar cells using fullerene derivatives [34, 35].

In this work HSC devices were fabricated with a bilayer structure of FTO/ $\text{TiO}_2$ /PTEBS/Au. ESD was compared to spin coating thin films of the water-soluble polymer PTEBS onto an interpenetrating  $\text{TiO}_2$  layer. Figure 2 shows an energy band diagram of the HSC devices fabricated. Light is absorbed by the PTEBS and an exciton is excited from the HOMO (–5.2 eV) to the LUMO (–3.2 eV) energy level [31]. The exciton is then separated into an electron and hole at the LUMO (–4.2 eV) of the  $\text{TiO}_2$  is [12]. The electron travels to the fluorine-doped tin oxide (FTO) (–4.4 eV) electrode and the hole goes to the gold (–5 eV) electrode [37, 38]. Average current densities were then modeled using the characteristic equation of an equivalent circuit of a solar cell.

## 2. Experimental

Transparent conductive FTO coated glass substrates of 12.5–14.5  $\Omega$  sheet resistance were purchased from Hartford Glass

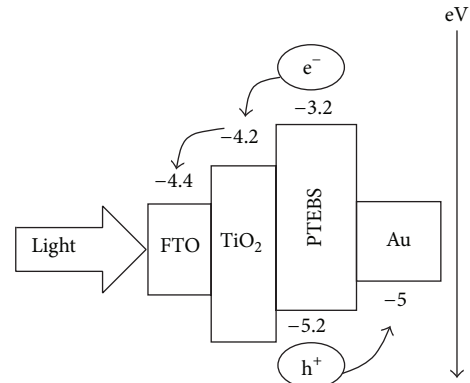


FIGURE 2: Energy band diagram of an HSC with a structure of FTO/ $\text{TiO}_2$ /PTEBS/Au.

Company. FTO substrates were then cleaned in ultrasonic baths of detergent, acetone, isopropanol, and water for 15 minutes each. Degussa P25  $\text{TiO}_2$  powder was suspended in 0.1M acetic acid by sonication for 12 hours. The  $\text{TiO}_2$  suspension was then left alone for 2 days to allow large particles to settle to the bottom before spin coating onto the FTO at 1700 rpm for 40 seconds to obtain a 2.1  $\mu\text{m}$  thick layer. The  $\text{TiO}_2$  was annealed for 1 hour at 500°C.

PTEBS was purchased from QCR solutions and dissolved in water at a 2% (by weight) concentration. The PTEBS layer was deposited by spin coating at 800 rpm to create a ~100 nm thick layer. Devices with a PTEBS layer from ESD were from a 0.5% solution in a water and ethanol blend with a 1:1 ratio before being loaded into a 1 mL syringe with a 30 G hypodermic needle. The ethanol cosolvent was used to lower the surface tension of the solution to maintain a steady Taylor cone for adequate film formation. Figure 3 illustrates a schematic of the electrospray configuration used to deposit PTEBS layers from ESD. The  $\text{TiO}_2$  coated FTO substrate was adhered to an aluminum plate with copper tape. The distance between the needle tip and the grounded aluminum plate holding the FTO substrate was 7 cm. The flow rate through the needle, controlled by a syringe pump, was 2  $\mu\text{L}/\text{min}$  and the applied voltage was 7.5–9 kV. The ITO substrate was grounded to the aluminum plate and sprayed for 1 hour to create a ~100 nm thick layer. The 80 nm thick gold electrodes were then deposited via sputter coating through a mask to create 0.06  $\text{cm}^2$  devices.

Device characterization was performed under 100  $\text{mW}/\text{cm}^2$  illumination using 1.5 AM light from a Spectra-Physics 96000 150 W Solar Simulator. Current and voltage source/measurements were obtained using a Keithley 236. A VEECO Icon Dimension AFMandan Ambios XP-1 profilometer was used to characterize films. A Hitachi Scanning Electron Microscope (SEM) was used to image  $\text{TiO}_2$  samples and measure pore sizes.

## 3. Modeling

A single diode electrical equivalent circuit (Figure 4) of a solar cell was used as a model to compute output current

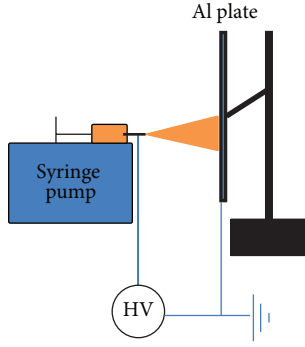


FIGURE 3: Schematic of ESD apparatus used in experiments.

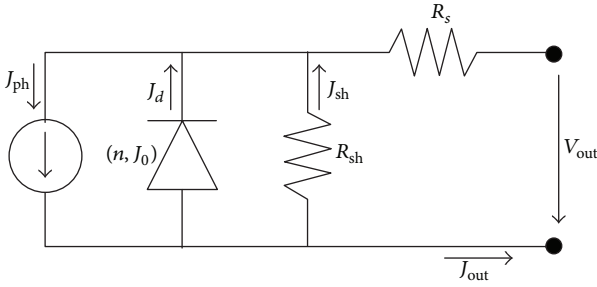


FIGURE 4: Equivalent circuit of a solar cell.

densities ( $J_{out}$ ). The equation describing the current-voltage characteristics of a solar cell is represented by

$$J_{out} = -J_0 \left[ \exp \left( \frac{V_{out} + R_s J_{out}}{nV_{th}} \right) - 1 \right] - \frac{V_{out} + R_s J_{out}}{R_{sh}} + J_{ph}, \quad (1)$$

where  $J_{out}$  is the output current density,  $J_0$  is the saturation current,  $V_{out}$  is the output voltage,  $R_s$  is the series resistance,  $n$  is the diode ideality factor,  $V_{th} = kT/q$  is the thermal voltage ( $k$  is the Boltzmann constant,  $T$  is the temperature, and  $q$  is the elementary charge),  $R_{sh}$  is the shunt resistance, and  $J_{ph}$  is the photocurrent. Equation (1) is a transcendental equation that expresses the current density output  $J_{out}$  as a function of itself and  $V_{out}$ . An explicit exact solution for (1) can be computed using the Lambert  $W$  function [39, 40]. Equation (1) must be expressed in the form of  $\omega e^\omega = x$  to utilize the Lambert  $W$  function, where

$$\omega = -\frac{R_s J_{out} + V_{out}}{nV_{th}} + \frac{R_s (J_0 + J_{ph}) + V_{out}}{nV_{th} (1 + G_p R_s)}, \quad (2)$$

$$x = \frac{R_s J_0}{nV_{th} (1 + G_p R_s)} \exp \left( \frac{R_s (J_0 + J_{ph}) + V_{out}}{nV_{th} (1 + G_p R_s)} \right),$$

where  $G_p = 1/R_{sh}$ . The solution to  $\omega e^\omega = x$  is the function Lambert  $W_k(x)$  where the branch ( $k$ ) of the solution corresponds to  $k = 0$  which satisfies Lambert  $W_0(x) = 0$ .

For simplification Lambert  $W = W$ , the explicit solution of (1) becomes [39, 40]:

$$J_{out} = -\frac{nV_{th}}{R_s} W \left[ \frac{R_s J_0}{nV_{th} (1 + G_p R_s)} \times \exp \left( \frac{R_s (J_0 + J_{ph}) + V_{out}}{nV_{th} (1 + G_p R_s)} \right) \right] - \frac{V_{out}}{R_s} + \frac{R_s (J_0 + J_{ph}) + V_{out}}{nV_{th} (1 + G_p R_s)}. \quad (3)$$

## 4. Results and Discussion

Table 1 displays the minimum, maximum, and average values of the short circuit current ( $J_{sc}$ ), open circuit voltage ( $V_{oc}$ ), and efficiency ( $\eta$ ) of 15 different HSC with PTEBS layers from ESD and spin coating. Figure 5 is a current density ( $J$ )-voltage ( $V$ ) plot of the average current density values of all devices for each construction type. The average  $J_{sc}$  for ESD devices was 0.0443 mA/cm<sup>2</sup> which was double the average  $J_{sc}$  of 0.0220 mA/cm<sup>2</sup> for spin coated devices. The average  $V_{oc}$  for ESD devices was 0.3406 V which was nearly half the average  $V_{oc}$  of 0.6493 V for spin coated devices. The average efficiency for ESD devices was 0.006%, slightly lower than the spin coated device efficiency of 0.0076%. The maximum efficiencies achieved from both device constructions were comparable at 0.009% but were significantly less than the highest reported identically structured spin coated devices of 0.17% [32]. The average standard deviation of the current densities was 0.0040 mA/cm<sup>2</sup> for the spin coated device construction and 0.0085 mA/cm<sup>2</sup> for the ESD device construction. ESD constructed devices have greater variations in morphology of the PTEBS layer which led to higher standard deviations and greater performance variation.

The substantial differences in  $J_{sc}$  and  $V_{oc}$  between the two different device constructions are likely due to the differences in the interfacial contact area between the TiO<sub>2</sub> and the PTEBS and the morphology of the PTEBS layer. Figure 6 is an SEM image of the TiO<sub>2</sub> interpenetrating network of nanoparticles. The average pore size is ~50 nm with a range of 10–100 nm.

When using the spin coating technique, the surface tension of the water inhibits the PTEBS solution from penetrating the nanopores of the TiO<sub>2</sub> layer. Incomplete or inadequate filling of porous TiO<sub>2</sub> nanostructures has been extensively reported as a deficiency in HSC [5, 6, 41–44]. By contrast, the ESD technique can lead to improved pore filling for two reasons. First, ESD generates particles small enough to penetrate the pores in the TiO<sub>2</sub> film. A histogram of particle diameters from ESD (Figure 7) reveals that the majority of PTEBS particles upon deposition are in the first bin, which ranges in diameter between 20 and 51.9 nm and has a median of 39.5 nm. The aerosolized polymer nanoparticles are able to penetrate the pores of the TiO<sub>2</sub> film and increase the interfacial contact area between the TiO<sub>2</sub>

TABLE 1: Table of minimum, maximum, and average values of short circuit current ( $J_{sc}$ ), open circuit voltage ( $V_{oc}$ ), and efficiency ( $\eta$ ) of 15 different HSC with electron donor layers from ESD and spin coating.

	Minimum			Average			Maximum		
	$J_{sc}$ (mA/cm <sup>2</sup> )	$V_{oc}$ (V)	$\eta$ (%)	$J_{sc}$ (mA/cm <sup>2</sup> )	$V_{oc}$ (V)	$\eta$ (%)	$J_{sc}$ (mA/cm <sup>2</sup> )	$V_{oc}$ (V)	$\eta$ (%)
ESD	0.0352	0.3400	0.0035	0.0443	0.3406	0.0060	0.0532	0.4200	0.0086
Spin	0.0186	0.5800	0.0060	0.0220	0.6493	0.0076	0.0245	0.7000	0.0088

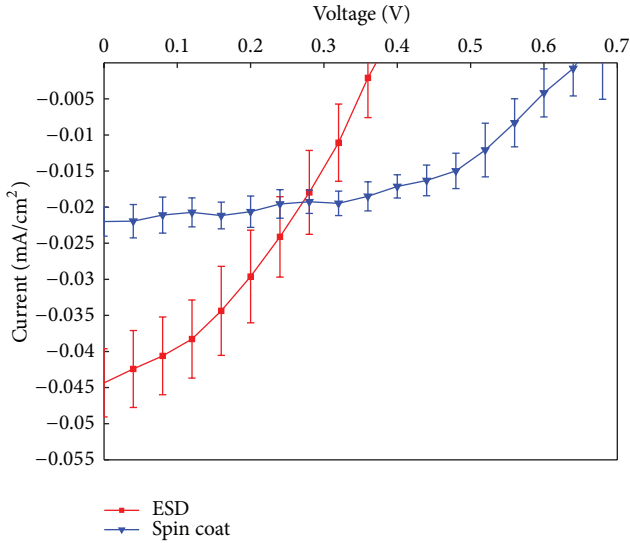


FIGURE 5: Average  $J$ - $V$  curves of 15 different devices from each deposition method of the PTEBS layer. The error bars show the standard deviation of the current along each measured voltage value.

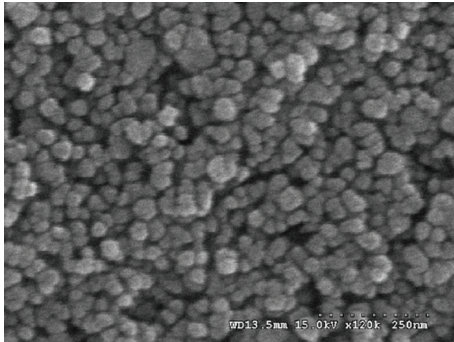


FIGURE 6: SEM image of the interpenetrating nanocrystalline  $\text{TiO}_2$  film at 120,000x magnification.

and PTEBS layers. In addition, the nanoparticles generated by ESD are electrically charged and are driven by the applied electric field. The electrostatic force also helps push the particles into the nanopores leading to improved interfacial contact area.

The ESD film includes interfacial boundaries between individual PTEBS particles that do not fully coalesce upon deposition. Kim et al. reported that these boundaries can diminish the performance of polymer solar cells [17]. Figure 8 is an AFM image of a PTEBS film from ESD showing that the

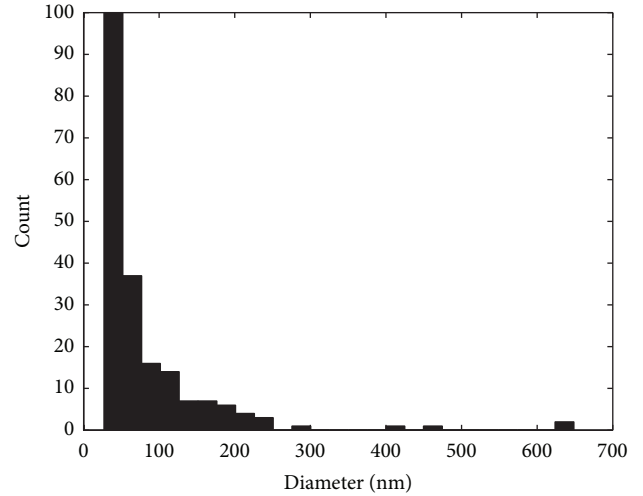


FIGURE 7: Histogram of particle diameters of a  $25 \mu\text{m}^2$  area after ESD for 3 minutes.

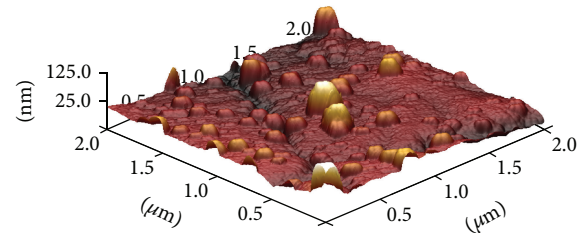


FIGURE 8: AFM image of PTEBS film from ESD.

film surface has some interfacial boundaries between particles even though it is a contiguous film. Film irregularities are believed to be the reason for a decrease in  $V_{oc}$ . The ESD film had a root mean squared surface roughness of 20.2 nm. The uniformity of a spin coated film as compared to an ESD film is a likely source for an increased standard deviation of output current density in devices with ESD construction.

The average  $J$ - $V$  curves from both coating techniques were then modeled using the characteristic equation of solar cells (see (1)). Figure 9 shows the model curves along with the average illuminated  $J$ - $V$  curves. The following parameter values used in the model were kept constant and agree with the previously reported values [45–47]:  $R_s = 4.2 \Omega$ ,  $R_{sh} = 100 \Omega$ ,  $n = 2.14$ ,  $k = 1.38 \times 10^{-23} \text{ J/K}$ ,  $q = 1.6 \times 10^{-19} \text{ C}$ , and  $T = 300 \text{ K}$ . The values of the series and shunt resistance were chosen because they gave the curves the proper shape. The reverse saturation current density ( $J_0$ ) and the photocurrent

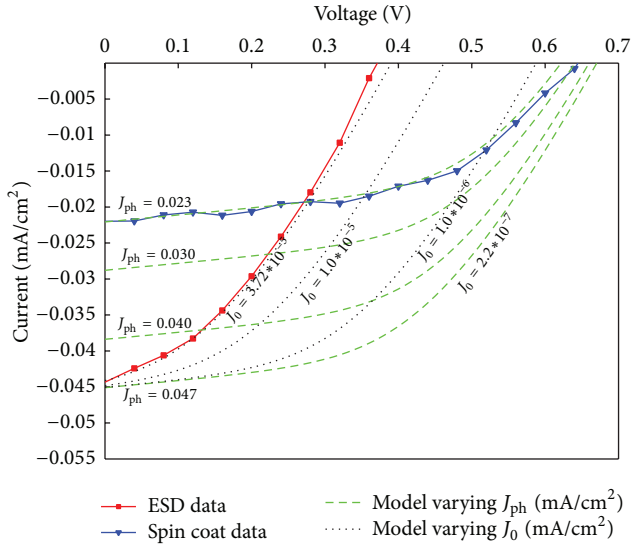


FIGURE 9: Illuminated average  $J$ - $V$  curves from experimental data and computational models. Model lines varying  $J_{ph}$  held a constant  $J_0 = 2.2 \times 10^{-7}$  mA/cm<sup>2</sup>. Model lines varying  $J_0$  held a constant  $J_{ph} = 0.047$  mA/cm<sup>2</sup>.

density ( $J_{ph}$ ) were used to fit the experimental curves. The spin coated  $J$ - $V$  curve agreed with the model at values of  $J_{ph} = 0.047$  mA/cm<sup>2</sup> and  $J_0 = 3.72 \times 10^{-5}$  mA/cm<sup>2</sup>, and the ESD  $J$ - $V$  curve agreed to the model with values of  $J_{ph} = 0.023$  mA/cm<sup>2</sup> and  $J_0 = 2.2 \times 10^{-7}$  mA/cm<sup>2</sup>. Increases in  $J_{ph}$  due to an increase in the interfacial contact area between the polymer and TiO<sub>2</sub> were also reported by Tanaka [48]. Our model shows that devices with PTEBS films from ESD generate double the amount of  $J_{ph}$ , and an increase of two orders of magnitude in the  $J_0$  compared to devices constructed from spin coating. The increase in  $J_0$  is attributed to poor film quality of ESD PTEBS films. The interfacial boundaries between PTEBS particles increase leakage current through the device sidewalls similar to decreasing  $R_{sh}$ , which is known to decrease  $V_{oc}$  [17, 39, 40, 49, 50]. Our model responds better by varying  $J_0$  rather than  $R_{sh}$  to demonstrate the effect of poor film quality on  $V_{oc}$ .

Figure 10 shows the dark  $J$ - $V$  curves of typical devices of each construction type along with the model curves. The  $J_0$  values in the model curves were the best fits ( $J_{0spin} = 3.72 \times 10^{-5}$  mA/cm<sup>2</sup> and  $J_{0ESD} = J_0 = 2.2 \times 10^{-7}$  mA/cm<sup>2</sup>) from the illuminated  $J$ - $V$  curves and  $J_{ph} = 0$  mA/cm<sup>2</sup>. The ESD model agrees very well with the experimental data while the spin coated model deviates slightly at higher voltages. However, the general trend of the model is largely in agreement with the experimental data.

## 5. Conclusions

ESD of the water-soluble polymer PTEBS thin films results in comparable efficiencies to traditional spin coating of thin films in TiO<sub>2</sub> solar cells. Devices produced from ESD generate nearly double the  $J_{sc}$  but approximately half the  $V_{oc}$  in

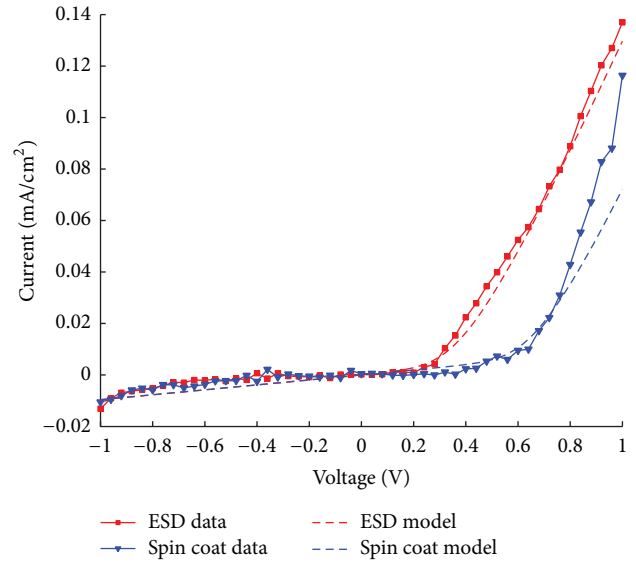


FIGURE 10: Dark  $J$ - $V$  curves of experimental data and model.

comparison to spin coated films. Devices from ESD have a larger standard deviation in current density due to greater variations in film morphology. The increase in  $J_{sc}$  is attributed to a greater interfacial contact area between the PTEBS and TiO<sub>2</sub> layers due to the superior penetration of electrospayed PTEBS droplets into the pores of the TiO<sub>2</sub>. Surface tension of the water prevents adequate penetration of the TiO<sub>2</sub>'s pores during spin coating. Poor film quality and surface roughness from interfacial boundaries between particles in the PTEBS layers from ESD are responsible for decreased  $V_{oc}$ . An exact analytic solution using the Lambert  $W$  function was used to model the experimental data from both devices construction types. The model showed an increase by a factor of 2 in  $J_{ph}$  in the ESD construction and an increase in  $J_0$  of two orders of magnitude in the ESD construction. The model also agreed with dark  $J$ - $V$  curves when  $J_{ph} = 0$  mA/cm<sup>2</sup>.

## Conflict of Interests

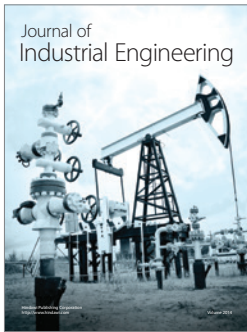
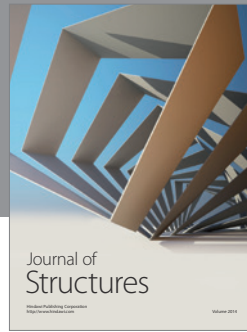
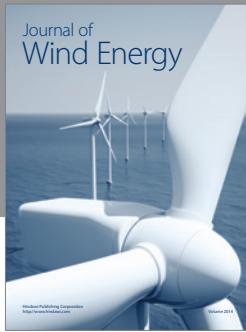
The authors declare that there is no conflict of interests regarding the publication of this paper.

## References

- [1] H. Hoppe and N. S. Sariciftci, "Morphology of polymer/fullerene bulk heterojunction solar cells," *Journal of Materials Chemistry*, vol. 16, no. 1, pp. 45–61, 2006.
- [2] D. Gebeyehu, C. J. Brabec, N. S. Sariciftci et al., "Hybrid solar cells based on dye-sensitized nanoporous TiO<sub>2</sub> electrodes and conjugated polymers as hole transport materials," *Synthetic Metals*, vol. 125, no. 3, pp. 279–287, 2002.
- [3] W. U. Huynh, J. J. Dittmer, and A. P. Alivisatos, "Hybrid nanorod-polymer solar cells," *Science*, vol. 295, no. 5564, pp. 2425–2427, 2002.
- [4] E. Hendry, F. Wang, J. Shan, T. F. Heinz, and M. Bonn, "Electron transport in TiO<sub>2</sub> probed by THz time-domain spectroscopy," *Physical Review B*, vol. 69, no. 8, Article ID 081101, 2004.

- [5] R. Könenkamp, "Carrier transport in nanoporous TiO<sub>2</sub> films," *Physical Review B*, vol. 61, pp. 57–64, 2000.
- [6] K. M. Coakley, B. S. Srinivasan, J. M. Ziebarth, C. Goh, Y. Liu, and M. D. McGehee, "Enhanced hole mobility in regioregular polythiophene infiltrated in straight nanopores," *Advanced Functional Materials*, vol. 15, no. 12, pp. 1927–1932, 2005.
- [7] A. J. Mozer and N. S. Sariciftci, "Negative electric field dependence of charge carrier drift mobility in conjugated, semiconducting polymers," *Chemical Physics Letters*, vol. 389, no. 4–6, pp. 438–442, 2004.
- [8] A. J. Mozer, N. S. Sariciftci, A. Pivrikas et al., "Charge carrier mobility in regioregular poly(3-hexylthiophene) probed by transient conductivity techniques: a comparative study," *Physical Review B*, vol. 71, no. 3, Article ID 035214, 2005.
- [9] H. Sirringhaus, N. Tessler, and R. H. Friend, "Integrated optoelectronic devices based on conjugated polymers," *Science*, vol. 280, no. 5370, pp. 1741–1744, 1998.
- [10] X. Yang, J. Loos, S. C. Veenstra et al., "Nanoscale morphology of high-performance polymer solar cells," *Nano Letters*, vol. 5, no. 4, pp. 579–583, 2005.
- [11] J.-M. Nunzi, "Organic photovoltaic materials and devices," *Comptes Rendus Physique*, vol. 3, no. 4, pp. 523–542, 2002.
- [12] A. J. Breeze, Z. Schlesinger, S. A. Carter, and P. J. Brock, "Charge transport in TiO<sub>2</sub>/MEH-PPV polymer photovoltaics," *Physical Review B*, vol. 64, no. 12, Article ID 125205, 2001.
- [13] A. M. Peiró, P. Ravirajan, K. Govender et al., "Hybrid polymer/metal oxide solar cells based on ZnO columnar structures," *Journal of Materials Chemistry*, vol. 16, no. 21, pp. 2088–2096, 2006.
- [14] D. Cheyns, K. Vasseur, C. Rolin, J. Genoe, J. Poortmans, and P. Heremans, "Nanoimprinted semiconducting polymer films with 50 nm features and their application to organic heterojunction solar cells," *Nanotechnology*, vol. 19, no. 42, Article ID 424016, 2008.
- [15] A. Jaworek and A. T. Sobczyk, "Electrospraying route to nanotechnology: an overview," *Journal of Electrostatics*, vol. 66, no. 3–4, pp. 197–219, 2008.
- [16] A. Jaworek, *Electrospray Technology for Thin-Film Deposition*, Nova Science Publishers, New York, NY, USA, 2010.
- [17] J.-S. Kim, W.-S. Chung, K. Kim et al., "Performance optimization of polymer solar cells using electrostatically sprayed photoactive layers," *Advanced Functional Materials*, vol. 20, no. 20, pp. 3538–3546, 2010.
- [18] T. Fukuda, K. Takagi, T. Asano et al., "Bulk heterojunction organic photovoltaic cell fabricated by the electrospray deposition method using mixed organic solvent," *Physica Status Solidi*, vol. 5, no. 7, pp. 229–231, 2011.
- [19] S.-E. Park, J.-Y. Hwang, K. Kim, B. Jung, W. Kim, and J. Hwang, "Spray deposition of electrohydrodynamically atomized polymer mixture for active layer fabrication in organic photovoltaics," *Solar Energy Materials and Solar Cells*, vol. 95, no. 1, pp. 352–356, 2011.
- [20] T. Fukuda, K. Takagi, and Y. Liao, "Insertion of fullerene layer for bulk heterojunction organic photovoltaic cell fabricated by electrospray deposition method," *Physica Status Solidi (RRL)*, vol. 7, pp. 1055–1058, 2013.
- [21] N. Ju, Y. Yamagata, and T. Higuchi, "Thin-film fabrication method for organic light-emitting diodes using electrospray deposition," *Advanced Materials*, vol. 21, no. 43, pp. 4343–4347, 2009.
- [22] V. Vohra, U. Giovanella, R. Tubino, H. Murata, and C. Botta, "Electroluminescence from conjugated polymer electrospun nanofibers in solution processable organic light-emitting diodes," *ACS Nano*, vol. 5, no. 7, pp. 5572–5578, 2011.
- [23] W. Hwang, G. Xin, M. Cho, S. M. Cho, and H. Chae, "Electrospray deposition of polymer thin films for organic light-emitting diodes," *Nanoscale Research Letters*, vol. 7, article 52, pp. 1–13, 2012.
- [24] T.-W. Zeng, H.-H. Lo, C.-H. Chang, Y.-Y. Lin, C.-W. Chen, and W.-F. Su, "Hybrid poly(3-hexylthiophene)/titanium dioxide nanorods material for solar cell applications," *Solar Energy Materials and Solar Cells*, vol. 93, no. 6–7, pp. 952–957, 2009.
- [25] P. Ravirajan, S. A. Haque, J. R. Durrant, D. D. C. Bradley, and J. Nelson, "The effect of polymer optoelectronic properties on the performance of multilayer hybrid polymer/TiO<sub>2</sub> solar cells," *Advanced Functional Materials*, vol. 15, no. 4, pp. 609–618, 2005.
- [26] D. Gebeyehu, C. J. Brabec, N. S. Sariciftci et al., "Hybrid solar cells based on dye-sensitized nanoporous TiO<sub>2</sub> electrodes and conjugated polymers as hole transport materials," *Synthetic Metals*, vol. 125, no. 3, pp. 279–287, 2002.
- [27] Q. Qiao, J. Beck, R. Lumpkin, J. Pretko, and J. T. Mcleskey Jr., "A comparison of fluorine tin oxide and indium tin oxide as the transparent electrode for P3OT/TiO<sub>2</sub> solar cells," *Solar Energy Materials and Solar Cells*, vol. 90, no. 7–8, pp. 1034–1040, 2006.
- [28] U.S. Department of Labor, Solvents—Safety and Health Topics—OSHA, 2007.
- [29] R. Søndergaard, M. Helgesen, M. Jørgensen, and F. C. Krebs, "Fabrication of polymer solar cells using aqueous processing for all layers including the metal back electrode," *Advanced Energy Materials*, vol. 1, no. 1, pp. 68–71, 2011.
- [30] N. S. Lewis and D. G. Nocera, "Powering the planet: chemical challenges in solar energy utilization," *Proceedings of the National Academy of Sciences of the United States of America*, vol. 103, no. 43, pp. 15729–15735, 2006.
- [31] Q. Qiao, L. Su, J. Beck, and J. T. McLeskey Jr., "Characteristics of water-soluble polythiophene: TiO<sub>2</sub> composite and its application in photovoltaics," *Journal of Applied Physics*, vol. 98, no. 9, Article ID 094906, 2005.
- [32] Q. Qiao, Y. Xie, and J. T. McLeskey Jr., "Organic/inorganic polymer solar cells using a buffer layer from all-water-solution processing," *Journal of Physical Chemistry C*, vol. 112, no. 26, pp. 9912–9916, 2008.
- [33] Q. Qiao and J. T. McLeskey Jr., "Water-soluble polythiophene-nanocrystalline TiO<sub>2</sub> solar cells," *Applied Physics Letters*, vol. 86, no. 15, Article ID 153501, 2005.
- [34] A. J. Miller, R. A. Hatton, and S. R. P. Silva, "Water-soluble multiwall-carbon-nanotube-polythiophene composite for bilayer photovoltaics," *Applied Physics Letters*, vol. 89, no. 12, Article ID 123115, 2006.
- [35] J. Yang, A. Garcia, and T.-Q. Nguyen, "Organic solar cells from water-soluble poly(thiophene)/fullerene heterojunction," *Applied Physics Letters*, vol. 90, no. 10, Article ID 103514, 2007.
- [36] QCR Solutions, Materials for Organic Solar Cells—PHT105A, 2010.
- [37] A. Andersson, N. Johansson, P. Bröms, N. Yu, D. Lupo, and W. R. Salaneck, "Fluorine tin oxide as an alternate to indium tin oxide in polymer LEDs," *Advanced Materials*, vol. 10, no. 11, pp. 859–863, 1998.
- [38] P. A. Anderson, "Work function of gold," *Physical Review*, vol. 115, no. 3, pp. 553–554, 1959.

- [39] S. Aazou and E. M. Assaid, "Modelling real photovoltaic solar cell using Maple," in *Proceedings of the 21th International Conference on Microelectronics (ICM '09)*, pp. 394–397, December 2009.
- [40] A. Jain and A. Kapoor, "Exact analytical solutions of the parameters of real solar cells using Lambert W-function," *Solar Energy Materials and Solar Cells*, vol. 81, no. 2, pp. 269–277, 2004.
- [41] L. Schmidt-Mende and M. Grätzel, "TiO<sub>2</sub> pore-filling and its effect on the efficiency of solid-state dye-sensitized solar cells," *Thin Solid Films*, vol. 500, no. 1-2, pp. 296–301, 2006.
- [42] H. Han, U. Bach, Y.-B. Cheng, and R. A. Caruso, "Increased nanopore filling: effect on monolithic all-solid-state dye-sensitized solar cells," *Applied Physics Letters*, vol. 90, no. 21, Article ID 213510, 2007.
- [43] P. Ravirajan, S. A. Haque, J. R. Durrant, D. D. C. Bradley, and J. Nelson, "The effect of polymer optoelectronic properties on the performance of multilayer hybrid polymer/TiO<sub>2</sub> solar cells," *Advanced Functional Materials*, vol. 15, no. 4, pp. 609–618, 2005.
- [44] A. F. Nogueira, C. Longo, and M.-A. De Paoli, "Polymers in dye sensitized solar cells: overview and perspectives," *Coordination Chemistry Reviews*, vol. 248, no. 13-14, pp. 1455–1468, 2004.
- [45] Y. Shen, K. Li, N. Majumdar, J. C. Campbell, and M. C. Gupta, "Bulk and contact resistance in P3HT:PCBM heterojunction solar cells," *Solar Energy Materials and Solar Cells*, vol. 95, no. 8, pp. 2314–2317, 2011.
- [46] P. Schilinsky, C. Waldauf, J. Hauch, and C. J. Brabec, "Simulation of light intensity dependent current characteristics of polymer solar cells," *Journal of Applied Physics*, vol. 95, no. 5, pp. 2816–2819, 2004.
- [47] G. del Pozo, B. Romero, and B. Arredondo, "Evolution with annealing of solar cell parameters modeling the S-shape of the current-voltage characteristic," *Solar Energy Materials and Solar Cells*, vol. 104, pp. 81–86, 2012.
- [48] S. Tanaka, "Performance simulation for dye-sensitized solar cells: toward high efficiency and solid state," *Japanese Journal of Applied Physics*, vol. 40, no. 1, pp. 97–107, 2001.
- [49] J. Song, Z. Xu, F. Zhang et al., "The effect of annealing treatment on the performance of bulk heterojunction solar cells with donor and acceptor different weight ratios," *Science in China G*, vol. 52, no. 10, pp. 1606–1610, 2009.
- [50] Y. Zhang, Z. Li, S. Wakim et al., "Bulk heterojunction solar cells based on a new low-band-gap polymer: morphology and performance," *Organic Electronics*, vol. 12, no. 7, pp. 1211–1215, 2011.



**Hindawi**

Submit your manuscripts at  
<http://www.hindawi.com>

